

CMB and Lyman- α constraints on dark matter decays to photons

Francesco Capozzi,^a Ricardo Z. Ferreira,^b Laura Lopez-Honorez^c
and Olga Mena^d

^aDipartimento di Scienze Fisiche e Chimiche, Universita degli Studi dell'Aquila, 67100 L'Aquila, Italy

^bInstitut de Física d'Altes Energies (IFAE) and Barcelona Institute of Science and Technology (BIST), Campus UAB, 08193 Bellaterra, Barcelona, Spain

^cService de Physique Theorique, Universite Libre de Bruxelles, C.P. 225, B-1050 Brussels, Belgium. Theoretische Natuurkunde & The International Solvay Institutes, Vrije Universiteit Brussel, Pleinlaan 2, B-1050 Brussels, Belgium

^dInstituto de Física Corpuscular (IFIC), University of Valencia-CSIC, Parc Científic UV, c/ Catedrático José Beltrán 2, E-46980 Paterna, Spain

E-mail: francesco.capozzi@univaq.it, rzambujal@ifae.es, Laura.Lopez.Honorez@ulb.be, omena@ific.uv.es

Abstract. Dark matter energy injection in the early universe modifies both the ionization history and the temperature of the intergalactic medium. In this work, we improve the CMB bounds on sub-keV dark matter and extend previous bounds from Lyman- α observations to the same mass range, resulting in new and competitive constraints on axion-like particles (ALPs) decaying into two photons. The limits depend on the underlying reionization history, here accounted self-consistently by our modified version of the publicly available **DarkHistory** and **CLASS** codes. Future measurements such as the ones from the CMB-S4 experiment may play a crucial, leading role in the search for this type of light dark matter candidates.

Contents

1	Introduction	1
2	Ionized fraction and IGM temperature evolution	2
2.1	Adiabatic cooling, Compton scattering and atomic processes	2
2.2	Dark matter energy injection and deposition	3
2.3	Reionization	4
2.3.1	The hyperbolic tangent function	4
2.3.2	Reionization from stars	5
3	CMB analysis	6
3.1	Energy deposition from $\text{DM} \rightarrow \gamma\gamma$ in CLASS	6
3.2	Current and future constraints for different reionization models	8
4	Lyman-α constraints	10
5	Conclusion	12
A	Rates	14
B	Modified DarkHistory	15

1 Introduction

Planck observations of the Cosmic Microwave Background Anisotropies (CMB) [1] constrain the cosmic ionization history while Lyman- α data, combined with state-of-the-art hydrodynamical simulations, have allowed precise determinations of the intergalactic medium (IGM) temperature at low-redshifts (see e.g. [2, 3] for recent analysis). These observations have then recently been used to search for the effects of annihilations and decays of Dark Matter (DM) particles that are known to modify both the ionization history and the temperature of the IGM throughout the universe’s history.

In this work, we revisit the imprints on the ionization history, from the recombination period until present times, and on the IGM temperature, at low redshifts ($z \lesssim 6$), for DM decays into two photons. We exploit Planck 2018 data to update previous CMB constraints on the 20.4 eV to keV mass range, and Lyman- α data to extend previous analyses for heavier DM masses to the same mass window, in which a plethora of axion-like particle (ALPs) DM models may lie.¹ The lower end of the mass range corresponds to twice the energy necessary for a Lyman- α transition in the Hydrogen atom: a photon with an energy below the Lyman- α threshold interacts with the gas much more weakly than a photon above the threshold, see e.g. [9, 10]. At the upper end, strong constraints from X-ray searches [11] dramatically prevent us to improve over the existing bounds with CMB and Lyman- α data.

For the CMB constraints, we will consider Planck 2018 data and extend the work of [11, 12] in a few ways. First, we take into account the energy injection efficiencies by making use of the **DarkHistory** code [13] and investigating the impact on the bounds of multiple reionization scenarios. We consider two well-motivated astrophysical models for the galactic UV/X-ray background [14, 15] and self-consistently take into account the DM feedback on the IGM temperature and on the ionization fractions by means of the use of **DarkHistory**. We then perform a full MCMC analysis in which we vary not only the relevant DM parameters but also other fiducial cosmological parameters, which can exhibit degeneracies, thus deriving robust bounds on both the DM mass and its coupling to photons.

¹See e.g. Refs. [4–8] for recent studies of ALP DM in this mass range.

We find bounds that can be competitive with those from the Leo-T dwarf galaxy [16]², when the astrophysical reionization model yields a relatively large optical depth to reionization. On the other hand, we show that CMB bounds are expected to become competitive to those of Leo-T with future CMB surveys, independently of the assumed reionization history.

Concerning the Lyman- α data analysis, we shall derive new bounds by extending the analysis provided in [17] to lower DM masses. We will follow the conservative approach proposed in Ref. [17], where robust constraints on DM from the IGM temperature were derived by fixing the reionization history to the Planck fiducial model and by neglecting the photoheating from astrophysical sources thus overcoming the large uncertainties associated to the astrophysical scenarios.

The structure of the manuscript is as follows. Section 2 contains a short description of the evolution of both the IGM temperature T_m and the free electron fraction x_e , including different reionization models. In Sec. 3, we introduce the treatment of the energy deposition efficiency that we then employ in our up-to-date CMB analysis to derive constraints on light DM decaying to photons with current data. In the same section, we also forecast how future CMB experiments will improve over the current constraints. Section 4 describes the analysis with Lyman- α data and the resulting constraints on the same DM decaying to photons scenario. Finally, we draw our conclusions in Sec. 5.

2 Ionized fraction and IGM temperature evolution

We start by briefly reviewing the different contributions to the evolution of the temperature of the intergalactic medium (IGM) T_m , and of the free electron fraction x_e . Here, we follow closely Refs. [13, 17], whose formalism has been implemented in the publicly available code `DarkHistory` [13]. This code allows to systematically solve for T_m and x_e including DM injections of energy all along recombination and reionization history as well as specific astrophysical models for the photoionization and photoheating rates at low redshifts. We will make use of `DarkHistory` (with some modifications) to obtain the results presented in Secs 3 and 4.

The evolution of the different ionization fractions is entangled with the evolution of the IGM temperature. The system of equations that keeps track of T_m and of the different contributions to x_e reads [18, 19]:

$$\dot{Y} = \dot{Y}^{(0)} + \dot{Y}^{\text{DM}} + \dot{Y}^{\text{astro}}, \quad \text{where } Y = \begin{pmatrix} T_m \\ x_{\text{HII}} \\ x_{\text{HeII}} \\ x_{\text{HeIII}} \end{pmatrix}, \quad (2.1)$$

where the ionized fractions x_X correspond to the ratios $x_X = n_X/n_H$ where n_H is the total Hydrogen density and $X = \text{HII}, \text{HeII}$ and HeIII stands for Hydrogen, singly ionized Helium and doubly ionized Helium, respectively.³ The contributions to the evolution of the temperature and ionized fractions are divided into three different terms. The first term $\dot{Y}^{(0)}$ accounts for adiabatic evolution, Compton scatterings and atomic processes, while the \dot{Y}^{DM} term is driven by DM energy injection in the medium. The third term \dot{Y}^{astro} is particularly relevant at low redshifts when astrophysics sources provide an extra source of photoionization and photoheating, triggering reionization. In Secs. 2.1 to 2.3 below, we briefly discuss each of these terms.

2.1 Adiabatic cooling, Compton scattering and atomic processes

Let us start by describing the $\dot{Y}^{(0)}$ term in Eq. (2.1). The corresponding contribution to the IGM temperature evolution reads [13, 17]:

$$\dot{T}_m^{(0)} = -2HT_m + \Gamma_C (T_{\text{CMB}} - T_m) + \dot{T}_m^{\text{atom}}. \quad (2.2)$$

²Gas-rich dwarf galaxies exhibit a behavior close to primitive galaxies in the early Universe and therefore they can be exploited as a tool to constrain non-standard cosmic ionization histories [16].

³Notice that at high redshifts the ionized Helium contributions can be neglected and the free electron fraction x_e reduces to the Hydrogen ionized fraction x_{HII} .

The first term accounts for adiabatic cooling whereas the second term describes Compton heating/cooling with Γ_C the Compton scattering rate, T_{CMB} the CMB temperature, and H is the Hubble rate. The last term includes multiple heating/cooling contributions due to atomic processes (recombination, collisional ionization, collisional excitation and bremsstrahlung) whose rates are given in Refs. [20, 21] (see also [17]). On the other hand, the evolutions of the ionized fractions is governed by

$$\dot{x}_X^{(0)} = \dot{x}_X^{\text{ion}} - \dot{x}_X^{\text{rec}}, \quad (2.3)$$

where \dot{x}_X^{ion} (\dot{x}_X^{rec}) accounts for ionization (recombination) processes. It is customary to discriminate between situations in which recombinations to the ground state are accounted for (case-A) or not (case-B), see e.g. [13, 21]. In our analysis, we follow [13] that treats redshifts below and above the onset of reionization (z_A^{max}) differently. At large redshifts compared to z_A^{max} , the universe is optically thin so case-B recombination and photoionization coefficients apply and the $\dot{x}_X^{(0)}$ term includes both contributions.⁴ In contrast, for $z \lesssim z_A^{\text{max}}$, the universe is more opaque to light and case-A recombination and collisional ionization contributions are instead taken into account (see [13, 20, 21] and Appendix A for the rates). Note that, at low redshifts, the photoionization rates are dominated by astrophysical contributions that are included in the \dot{Y}^{astro} term of Eq. (2.1) (see the discussion in Sec. 2.3.2).

Finally, we briefly comment on a modification in the matter temperature evolution considered in our analysis compared to the default implementation in **DarkHistory**. In the latter code, collisional excitation processes are only included at low redshift, after recombination starts. We found, however, that this is not a good approximation for light dark matter masses below $\mathcal{O}(100)$ eV (see Appendix B and Fig. 8). Therefore, we have modified the code to include the effect of collisional excitation at all times for the matter temperature evolution.

2.2 Dark matter energy injection and deposition

The \dot{Y}^{DM} term of Eq. (2.1) accounts for the dark matter annihilation/decay contributions. To describe this term, let us focus on an ALP dark matter particle a of mass m_a that decays into two photons of energy $m_a/2$ at a rate $\Gamma_{\text{dec}} \gg t_0^{-1}$ (where t_0 is the age of the universe). The energy injected per unit of time and volume is given by

$$\left(\frac{dE(z)}{dt dV} \right)_{\text{injected}} = \rho_a (1+z)^3 \Gamma_{\text{dec}}, \quad (2.4)$$

where ρ_a is the energy density of the DM particle today and the decay rate is parametrized as

$$\Gamma_{\text{dec}} = g_{a\gamma\gamma}^2 m_a^3 / (64\pi), \quad (2.5)$$

with $g_{a\gamma\gamma}$ the ALP-photon coupling. In the next sections, we will phrase our constraints on DM decays to photons in terms of the ALPs parameters m_a and $g_{a\gamma\gamma}$. Note however that, by properly re-expressing the bounds on $g_{a\gamma\gamma}$ in terms of the DM lifetime Γ_{dec}^{-1} , our constraints apply to any DM model decaying to two photons.

The injected energy may not be deposited instantaneously into the medium due to the cooling of primary particles. In addition, there are multiple channels c of energy deposition including IGM heating (denoted with $c = \text{heat}$), Hydrogen ionization ($c = \text{HII}$), Helium single or double ionization ($c = \text{HeII}$ or HeIII), and neutral atom excitation ($c = \text{exc}$). The fraction of energy injected that is deposited in the different channels can be expressed as [22]

$$\left(\frac{dE_c(x_e, z)}{dt dV} \right)_{\text{deposited}} = f_c(x_e, z) \left(\frac{dE(z)}{dt dV} \right)_{\text{injected}}, \quad (2.6)$$

where the coefficients, $f_c(x_e, z)$, are the DM energy deposition efficiencies. They account for all the details associated to the delay in energy deposition and separation into different channels c at a given redshift z and free electron fraction x_e (that is a function of the different ionization fractions x_X).⁵

⁴In an optically thin medium, photons of 13.6 eV, arising from recombinations to the H ground state, are absorbed in much less than a Hubble time and Hydrogen cannot recombine in this way. In the latter case, only case-B recombination coefficients shall be taken into account.

⁵In practice, f_c depends on each of the ionization fraction $x_H, x_{\text{HeII}}, x_{\text{HeIII}}$ independently [13].

We make use of **DarkHistory** [13] to obtain the $f_c(x_e, z)$ functions. In the **DarkHistory** code, the term \dot{Y}^{DM} in Eq. (2.1) takes the form:

$$\dot{Y}^{\text{DM}} = A \times \frac{1}{n_{\text{H}}} \left(\frac{dE(z)}{dt dV} \right)_{\text{injected}}, \quad (2.7)$$

where the prefactor $A = A(f_c(x_e, z))$ is a function of the deposition fractions $f_c(x_e, z)$ (see Appendix A and Ref. [17] for details).

2.3 Reionization

At low redshifts, typically at $z \lesssim z_A^{\text{max}}$, star formation and active galactic nuclei are expected to inject extra sources of energy in the IGM and to drive reionization at $z = z_{\text{reio}} < z_A^{\text{max}}$, see e.g. the discussion in Refs. [23, 24]. Here, we will consider two different approaches to reionization. We begin with a description of the canonical hyperbolic tangent model in Sec. 2.3.1. The latter provides an effective parametrization of the ionized fraction at low z . We then describe in Sec. 2.3.2 two well-motivated reionization scenarios that rely on different models of UV and X-ray background emission from galaxy formation processes and give rise to distinct photoionization and photoheating rates. The latter are necessary to make a self-contained evolution of both the free electron fraction, x_e , and the IGM temperature, T_m , at low z . Their effect is taken into account in the \dot{Y}^{astro} term of Eq. (2.1). The corresponding ionized fractions and, when relevant, temperature evolutions, are illustrated in Fig. 1 around the epoch of reionization for each of the models. In our CMB analysis of Sec. 3, we study the impact of the ionized fraction x_e evolution, obtained for the three different reionization models, on the CMB anisotropies. In Sec. 4, when computing the Lyman- α constraints on T_m , we will instead be interested in deriving conservative bounds on the amount of DM heating thus, following [17], we neglect the astrophysical sources of heating at low redshifts and fix the ionized fraction at low redshifts to the hyperbolic tangent model.

A useful quantity when comparing different reionization histories is the optical depth to reionization, τ , that we define as

$$\tau = \int_0^{z_{e,\text{min}}} dz n_e \sigma_T \frac{dt}{dz}, \quad (2.8)$$

i.e. the integral, between today and the time at which the electron fraction displays a minimum (tagged as $z_{e,\text{min}}$), of the free electron number density⁶, $n_e(z)$, multiplied by the Thompson cross-section, σ_T . This is the prescription followed in the publicly available **CLASS** Boltzmann solver code [25–27].⁷

2.3.1 The hyperbolic tangent function

The most widely used model for the reionization history exploits the hyperbolic tangent function [28]:

$$x_e^{\text{tanh}}(z) = \frac{1 + \mathcal{F}_{\text{He}}}{2} \left(1 + \tanh \left[\frac{y(z_{\text{reio}}) - y(z)}{\Delta_y} \right] \right), \quad (2.9)$$

where $\mathcal{F}_{\text{He}} = n_{\text{HeII}}/n_{\text{H}}$ is the ratio of singly ionized Helium to Hydrogen atoms⁸, $y(z) = (1+z)^\gamma$, $\Delta_y = \gamma(1+z_{\text{reio}})^{\gamma-1}\Delta_z$, where Δ_z is the width of the transition. The parameters Δ_z and γ are the are fixed to 0.5 and 3/2 respectively. The only free parameter that we will vary here is the reionization redshift z_{reio} . With such a reionization model, Planck 2018 temperature and polarization data gives rise to an optical depth to reionization

$$\tau_{\text{Pl}} = 0.054 \quad \text{with} \quad \sigma_{\text{Pl}}(\tau) = 0.007 \quad (2.10)$$

⁶ $n_e(z) = x_e(z)n_{\text{H}}(z)$, where n_{H} is the Hydrogen density.

⁷Other prescriptions might have defined a default maximum redshift. In the case of e.g. extended reionization histories or exotic energy injection, an arbitrary choice of maximum redshift strongly affect the value of τ while the prescription used in Eq. (2.8) is nearer to what Planck data is effectively sensitive to, see the discussion in Ref. [24].

⁸The contribution from doubly ionized Helium to the free electron fraction is added in the form of another hyperbolic tangent but at lower redshift, $z \sim 3.5$, when HeII is expected to be ionized [1].

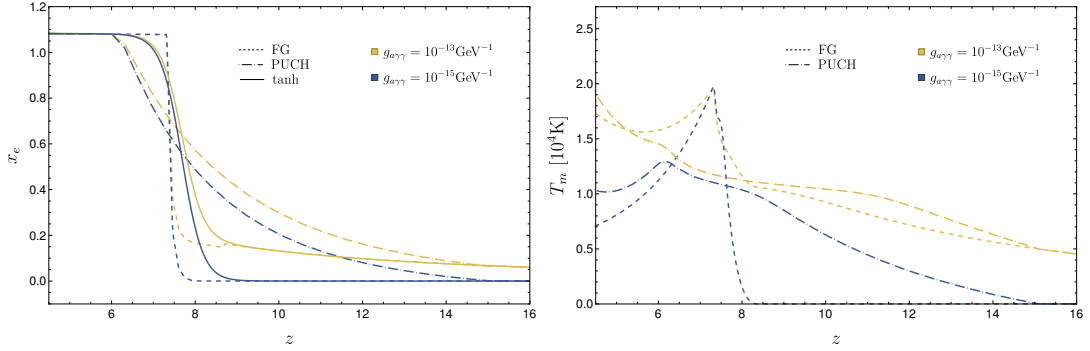


Figure 1. Ionisation and IGM temperature histories for different reionization models including the energy injections from the decays into two photons of a DM particle of mass $m_a = 95$ eV and two different couplings to photons. On the left panel, we focus on the free electron fraction illustrating with blue and orange curves the reionization models of FG (dashed lines), PUCH (dot-dashed lines) and hyperbolic tangent (solid lines) for $z_{\text{reio}} = 7.68$ (continuous) and consider DM energy injection for two possible values of the DM-photon coupling $g_{a\gamma\gamma} : 10^{-15}$ and $10^{-13} \text{ GeV}^{-1}$. The right panel depicts the matter temperature evolution in redshift for the very same two astrophysical-based reionization models and couplings $g_{a\gamma\gamma}$.

where $\sigma_{\text{PI}}(\tau)$ denotes the 68% CL error [1]. This implies a mid-point redshift of reionization $z_{\text{reio}} = 7.68 \pm 0.79$ at 68% CL, suggesting that the Universe was fully reionized by $z \simeq 6$. The interest in this model is justified by the fact that it is easy to explore a large set of reionization histories by varying z_{reio} or even the reionization width. In the left panel of Fig. 1, the continuous curves illustrate the ionized fraction evolution within an hyperbolic tangent model assuming $z_{\text{reio}} = 7.68$. The blue curve assumes a negligible energy injection from DM decays and is in agreement with Planck 2018 data. The yellow curve is obtained with a larger coupling to photons affecting the ionization history at $z \gtrsim z_{\text{reio}}$.

2.3.2 Reionization from stars

Apart from the hyperbolic tangent model, in this paper, we shall also consider two explicit reionization models from Puchwein et al. [15] and Fauchere-Giguère [14], that we denote by PUCH and FG, respectively, for short.⁹ Those reionization scenarios rely on observations of the UV and X-ray background emission from galaxies to model the photoionization ($\Gamma_X^{\gamma\text{-ion}}$) and photoheating ($\mathcal{H}_X^{\gamma\text{-heat}}$) rates from astrophysical sources contributing to the \dot{Y}^{astro} term of Eq. (2.1) as [13, 17]

$$\begin{pmatrix} \dot{T}_m^{\text{astro}} \\ \dot{x}_X^{\text{astro}} \end{pmatrix} = \begin{pmatrix} \frac{2}{3(1+\mathcal{F}_{\text{He}}+x_e)n_{\text{H}}} \sum_X \mathcal{H}_X^{\gamma\text{-heat}} \\ x_X \Gamma_X^{\gamma\text{-ion}} \end{pmatrix} \quad (2.11)$$

where $X=\{\text{HII}, \text{HeII}, \text{HeIII}\}$.

There are several differences between the PUCH and FG models. First, the onset of reionization, z_A^{max} , is given by $z_{\text{PUCH}}^{\text{max}} = 15.1$ and $z_{\text{FG}}^{\text{max}} = 7.8$ for the PUCH and FG reionization models, respectively. Moreover, in the FG model reionization is relatively rapid compared to the PUCH model. These differences are illustrated in Fig. 1, where we depict the redshift evolution of x_e (left panel) and T_m (right panel) with a dashed line for the FG model and a dot-dashed line for the PUCH model. Let us emphasize that, for redshifts above z_A^{max} and fixed values of the coupling to photons, all $x_e(z)$ and $T_m(z)$ curves are identical by construction. Indeed, the \dot{Y}^{astro} term only accounts for extra energy injection from stars at $z < z_A^{\text{max}}$.

In the left panel of Fig. 1, where we show the evolution of the free electron fraction as a function of the redshift, we consider a DM particle with 95 eV mass and two distinct couplings to photons (see Eq. (2.5)), $g_{a\gamma\gamma} = 10^{-15} \text{ GeV}^{-1}$ (blue lines) and $g_{a\gamma\gamma} = 10^{-13} \text{ GeV}^{-1}$ (orange lines), that correspond,

⁹The PUCH model is implemented by default in **DarkHistory** while we have implemented the FG model by making use of the tabulated photoheating and photoionization rates provided [here](#).

respectively, to a negligible and a significant DM energy injection. After implementing the PUCH and FG models in `DarkHistory` and using Eq. (2.8) to evaluate the optical depth, we obtain for the default PUCH and FG reionization models (i.e. the blue curves with negligible DM energy injection):¹⁰

$$\tau_{\text{PUCH}} = 0.064, \quad \text{and} \quad \tau_{\text{FG}} = 0.052. \quad (2.12)$$

Comparing these optical depths to the one reported by Planck in Eq. (2.10), it is clear that the FG reionization model will lead to more conservative bounds on the DM scenario than the PUCH model. Indeed, the latter gives rise to a larger optical depth to reionization leaving less room for an extra DM contribution to the free electron fraction.

The IGM temperature evolution is depicted in the right panel of Fig. 1. We show in blue (orange) an ALP-photon coupling of $g_{a\gamma\gamma} = 10^{-15} \text{ GeV}^{-1}$ ($g_{a\gamma\gamma} = 10^{-13} \text{ GeV}^{-1}$) and the dashed and dot-dashed curves show the IGM temperature evolution in the PUCH and FG models. We clearly see the differences between these two reionization models as well as the impact of DM energy injection. In all cases, the DM decay into photons induces higher IGM temperature for larger couplings to photons (well visible for $z > z_{\text{PUCH}}^{\text{max}}$). Also, for both PUCH and FG models, we see the presence of a bump in the IGM temperature that roughly starts at the onset of reionization and peaks when the latter is completed. In the PUCH model, the changes in the IGM temperature are smoother as reionization starts at higher redshifts than in the FG case. In the FG model, reionization happens on a much shorter time scale, the changes are more abrupt and cause a sharper peak in the evolution of the matter temperature at reionization ($z \simeq 8$). Notice though that the values of T_m on this peak of temperature remain at most within a factor ~ 2 from the values of T_m in the $z < 6$ redshift range, where current observations of the IGM temperature are relevant.

3 CMB analysis

As discussed in the previous sections, energy injection from annihilations or decays of DM particles in the early universe can leave a detectable imprint on CMB anisotropies, see e.g. [10, 22, 29, 30], that can lead to strong constraints on beyond the Standard Model scenarios, see e.g. [11, 12, 17, 23, 31–33]. The energy injection efficiencies and the different reionization histories, discussed in Secs 2.2 and 2.3, are two crucial inputs for our CMB analysis. In this section, we first discuss in Sec. 3.1 how in practice we deal with energy injection from DM and stars in the public CMB Boltzmann solver code `CLASS`. Based on this approach, we then present in Sec. 3.2 the results of a Monte Carlo Markov Chain (MCMC) analysis that provides updated constraints on the DM parameter space using the CMB temperature and polarization measurements by Planck 2018. Finally, we end the section with the prospects to constrain the DM coupling to photons with future CMB measurements by using the forecasted sensitivities in the measurement of the optical depth to reionization.

3.1 Energy deposition from $\text{DM} \rightarrow \gamma\gamma$ in `CLASS`

The `CLASS` Boltzmann solver [26, 34] can account for exotic energy injection at high redshifts ($z \gtrsim z_{\text{reio}}$) building upon the `ExoCLASS` extension, see Refs. [35, 36]. In the case of DM decays, the default implementation in the `injection` module fixes the energy deposition efficiencies $f_c(x_e, z)$ to those given in Ref. [30], which essentially reduce to $f_c(x_e, z) = 1/3$ for $c = \text{HII}$, heat and exc at large z . At $z \lesssim z_{\text{reio}}$ the ionized fraction follows by default the hyperbolic tangent model presented in Sec. 2.3.1. The `thermodynamics` module allows however to implement any reionization history by providing a list of $x_e(z)$ points between which `CLASS` interpolates.

In order to efficiently account for a more accurate treatment of energy deposition from dark matter and stars, we have made slight modifications of both the `injection` and `thermodynamics` modules of `CLASS`.¹¹

¹⁰The very same results can be obtained by implementing these two reionization histories in `CLASS` with the `reio_parametrization` set to `reio_inter` that takes into account tabulated values of (z, x_e) between $z = 6$ and $z_{\text{PUCH}}^{\text{max}} = 15.1$ and $z_{\text{FG}}^{\text{max}} = 7.8$ for PUCH and FG reionization models explicitly. Notice that our result for τ_{FG} differs from the reported value by [14] by 0.002. This might be due to a slight difference in the prescription for computing τ .

¹¹Our modified version of `CLASS` is available at the following link: https://github.com/llopezho/CLASS_DMdecay.

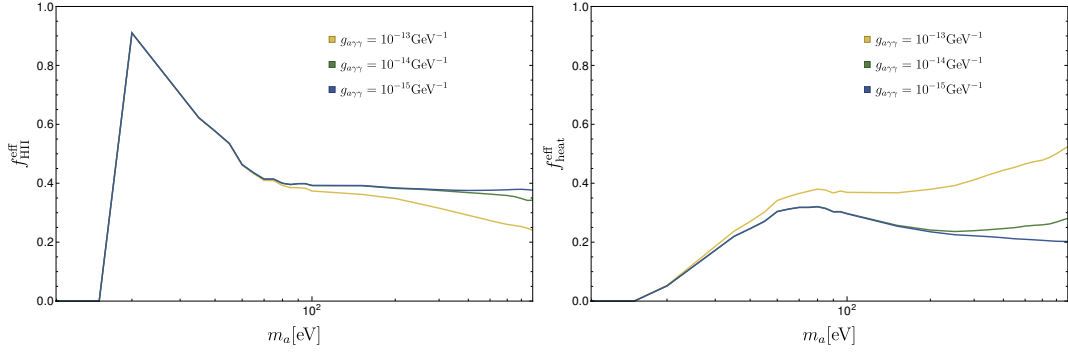


Figure 2. *Effective energy deposition efficiencies* dependence on the DM mass and coupling to photons. The plots illustrate the case of energy deposition into Hydrogen ionization ($c = \text{HII}$, left panel) and heating of the IGM ($c = \text{heat}$, right panel) as a function of m_a , in the mass range considered in our analysis, for couplings $g_{a\gamma\gamma} = 10^{-15}$ (in blue), 10^{-14} (in green) and $10^{-13} \text{ GeV}^{-1}$ (in orange). Those efficiencies are used in our CMB analysis at $z > z_A^{\text{max}}$, see text for details.

- At $z \lesssim z_A^{\text{max}}$, we account for specific reionization from stars (PUCH or FG models) interpolating, within the `thermodynamics` module, a tabulated evolution of $x_e(z)$ between $z = 6$ and z_A^{max} for different values of the DM parameters m_a and $g_{a\gamma\gamma}$ within the ranges of interest, see Sec. 3.2. These tabulated values have been obtained with `DarkHistory` and take into account the convoluted effect of DM decay and reionization from stars.
- Before reionization, we have made use of an approximation to the energy deposition, described in Eq. (2.6), that facilitates the computation of energy injection efficiencies for any DM mass and couplings relevant here. We discuss the latter in more detail below. Let us also mention that in all cases we have made use of the default `HyRec` recombination algorithm [37, 38]

It is well known that in the case of dark matter decays, efficient energy deposition is delayed to later times with respect to e.g. the annihilating DM case, see for example the discussion in Refs. [10, 17, 31–33]. In Ref. [33], it was shown by means of a principal component analysis that the impact of DM decays on the CMB (between reionization and recombination) is well captured using the energy deposition efficiencies $f_c(x_e, z)$ at redshift $z \simeq 300$, as expected from the results of Ref. [39]. This allows to shortcut the treatment of high redshift energy deposition by using:

$$\left(\frac{dE_c(x_e, z)}{dt dV} \right)_{\text{deposited}} = f_c^{\text{eff}} \left(\frac{dE(x_e, z)}{dt dV} \right)_{\text{injected}} \quad \text{for } z > z_A^{\text{max}}, \quad (3.1)$$

where $f_c^{\text{eff}} = f_c(x_e, z = 300)$ is used as an effective energy deposition efficiency parameter. In our CMB analysis, we use this approximation at high redshifts instead of the full $f_c(x_e, z)$ treatment of Eq. (2.6). In Fig. 2, we illustrate the dependence of $f_{\text{HII,heat}}^{\text{eff}}$ on the dark matter mass for different values of the coupling to photons (or equivalently of lifetimes). We see that for $m_a \lesssim \mathcal{O}(100) \text{ eV}$, ionization becomes the main channel for energy deposition at large redshifts, except below $m_a < 26 \text{ eV}$ where the excitation channel is dominant.

In Ref. [33], it was explicitly checked that f_c^{eff} is in excellent agreement with the first principal component of $f_c(x_e, z)$ for decaying DM masses above 10^4 eV . Making use of the `DarkHistory` package and of our modified `CLASS` code, we found an excellent agreement on $x_e(z)$ when comparing the effective or the full energy deposition approaches for $z_{\text{reio}} < z < 10^3$ and dark matter masses between 20.4 eV and 10^4 eV . This is illustrated in Fig. 3 where we focus on a dark matter particle with a mass $m_a = 95 \text{ eV}$ decaying into two photons with a coupling $g_{a\gamma\gamma}$ between $10^{-13} \text{ GeV}^{-1}$ (orange lines) and $10^{-15} \text{ GeV}^{-1}$ (blue lines) and assuming a PUCH reionization model. The continuous colored lines are obtained with the `DarkHistory` software using the full treatment of $f_c(x_e, z)$, as in Eq. (2.6), while

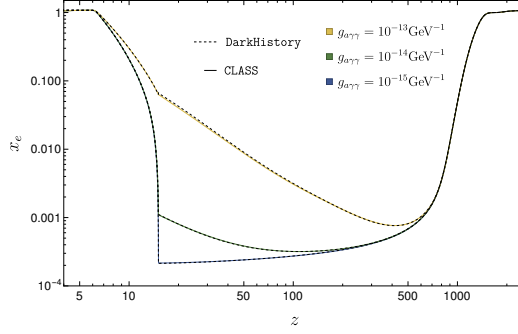


Figure 3. Comparison of the different numerical approaches when considering the dark matter energy injections through decays of a dark matter particle of mass $m_a = 95$ eV and different couplings and reionization models. On the left panel, we depict the ionization history when considering a PUCH reionization model in our modified version of the CLASS Boltzmann package code (dashed lines) and that recovered from the full treatment of the DarkHistory package (continuous colored lines) for couplings $g_{a\gamma\gamma} = 10^{-15}$ (in blue), 10^{-14} (in green) and 10^{-13} GeV^{-1} (in orange).

the dashed lines are obtained with the CLASS code, making use of the effective energy deposition of Eq. (3.1) with $f_c^{\text{eff}} = f_c(x_e, z = 300)$ from DarkHistory. Notice that continuous and dashed lines are almost identical as expected.

3.2 Current and future constraints for different reionization models

Based on the prescription for energy injection at recombination and reionization described in Sec. 3.1, we now use Planck 2018 data to derive constraints on sub-keV decaying dark matter. We present the bounds in the plane of the DM mass m_a and DM coupling to photons $g_{a\gamma\gamma}$, that effectively set the decay rate (see Eq. (2.5)). We focus on the mass and coupling ranges:

$$m_a \supset [10, 10^4] \text{ eV} \quad \text{and} \quad \log_{10}[g_{a\gamma\gamma} \times \text{GeV}] \supset [-12, -16]. \quad (3.2)$$

We also analyse the impact of the underlying reionization model on the constraints. More precisely, we derive the bounds that arise in the case of the hyperbolic tangent reionization model of Sec. 2.3.1, denoted by tanh for short, and compare them to the explicit FG and PUCH astrophysical models presented in Sec. 2.3.2.

Before going through the detailed statistical analysis, we can infer a first rough estimate of the expected bounds in the case of the PUCH and FG models. To that purpose, we compute with our modified version of CLASS the optical depth to reionization over the whole range of $(m_a, g_{a\gamma\gamma})$ reported in 3.2 and estimate the bounds by excluding the region where $\tau > \tau_{\text{P1}} + 2 \times \sigma_{\text{P1}}$. The corresponding limits are shown with dashed and dot-dashed gray lines in Fig. 4 for the FG and PUCH reionization models, respectively. The expected excluded regions at 2σ CL lie above those gray lines. Notice that the PUCH model gives rise to stronger constraints, as anticipated in Sec. 2.3.2. Indeed even without dark matter energy injection, the PUCH model yields an optical depth, $\tau = \tau_{\text{PUCH}}$, that is more than 1σ above the central value preferred by the Planck 2018 data. Including DM energy injection, the limit on $g_{a\gamma\gamma}$ for fixed m_a in the PUCH model is roughly half an order of magnitude stronger than in the FG case.

We can now perform a full Monte Carlo analysis. The minimal set of cosmological parameters considered in our analysis includes:

$$\{\Omega_b h^2, \Omega_c h^2, 100\theta_*, \ln[10^{10} A_s], n_s, \log_{10}[m_a/\text{eV}], \log_{10}[g_{a\gamma\gamma} \times \text{GeV}]\}. \quad (3.3)$$

In the case of the PUCH and FG reionization models we work with fixed photoionization and photo-heating rates and thus perform the MCMC on the set of parameters (3.3). In contrast, in the case of the hyperbolic tangent model, the set of parameters is supplemented by the reionization redshift z_{reio} .

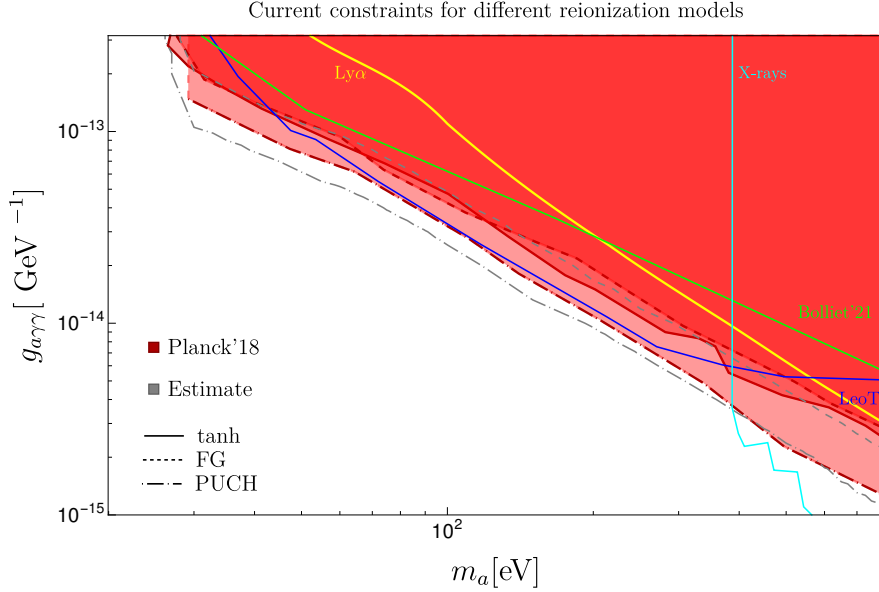


Figure 4. Exclusion limits from CMB anisotropies in the $(m_a[\text{eV}], g_{a\gamma\gamma}[\text{1/GeV}])$ plane. The red lines correspond to the regions excluded at 99% CL from Planck 2018 data for different reionization histories: the standard hyperbolic tangent description (continuous), the Fauchere-Giguère (FG) model (dashed) and the Puchwein (PUCH) model (dot-dashed). In the case of FG and PUCH models, the corresponding gray lines show a rough estimate of the exclusion limits based on the evaluation of the optical depth to reionization. The yellow continuous line represents the most stringent constraint derived in Sec. 4 from Lyman- α data assuming a tanh reionization. The other continuous colored lines correspond to existing limits from a previous CMB analysis [12] (green), X-ray analysis [11] (cyan) as well as the conservative constraint from Leo-T [16] (blue).

In the latter case, we can thus effectively marginalize over multiple reionization scenarios. In Eq. (3.3), $\Omega_b h^2$ and $\Omega_a h^2$ are the relative baryon and decaying dark matter densities today, θ_* is the acoustic scale angle and A_s and n_s are, respectively, the amplitude and spectral index of the primordial power spectrum. For the latter purposes, we have run the `MontePython` software [40] interfaced with our modified version of `CLASS` and used the baseline TT, TE, EE + lowE Planck 2018 likelihoods. The resulting bounds at 99% CL are depicted in Fig. 4 in thick red continuous, dashed and dot-dashed lines for, respectively, the tanh, FG and PUCH reionization models. Interestingly, we notice that the results of the Monte Carlo analysis are in good agreement with the estimated bounds (gray lines). In addition, we note that the tanh model, marginalizing over the reionization redshift in the range $z_{\text{reio}} = 5$ to 13, leads to a constraint on the parameter space that is very similar to the conservative case of a FG reionization scenario. We also note that we have not found any clear degeneracy between the DM parameters and any of the cosmological parameters in the analysis.

The CMB bounds derived here are more stringent than the previous ones from [11, 12]. Indeed, our analysis differs from the previous ones in a few aspects. First, we use a more recent CMB data release, which translates into a lower value of τ . Second, we make use of more accurate values for the energy deposition efficiency coefficients by including the $f_c(x_e, z = 300)$ computed from `DarkHistory` and we exploit the full CMB anisotropy spectrum information rather than just the optical depth to reionization. Also, we perform a full MCMC analysis to extract the constraints from CMB anisotropies. Let us also emphasize that our bounds are competitive with the constraints from the radiative cooling gas rate of the Leo-T dwarf galaxy [16] in the case of the more aggressive PUCH reionization scenario.

Concerning future prospects, CMB-S4 surveys are expected to reach a 1σ uncertainty on the optical depth to reionization of $\sigma(\tau) = 0.0025$ [41]. Preliminary estimates also show that by combining measurements of the kinematic Sunyaev-Zeldovich (kSZ) effects with the CMB-S4 data, the sensitivity

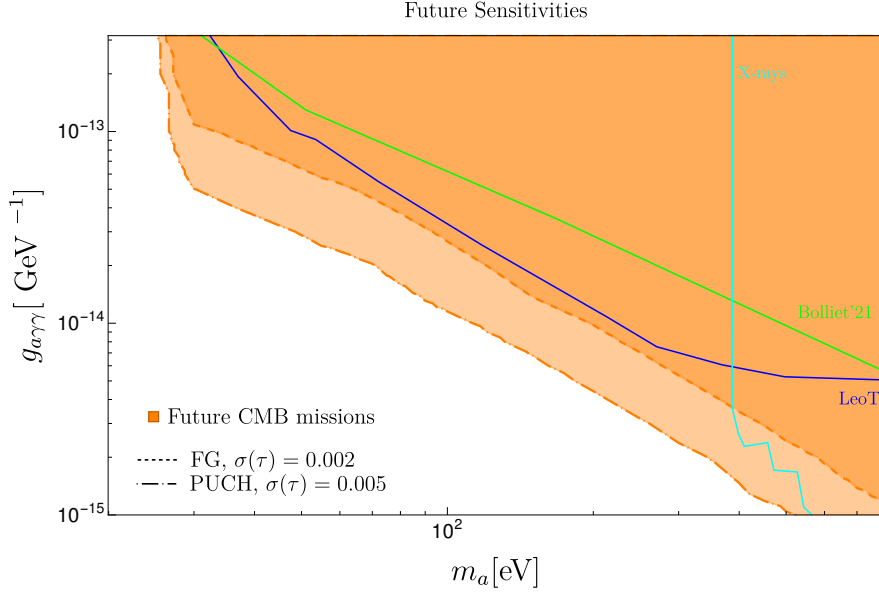


Figure 5. Sensitivities of future CMB missions. The orange lines correspond to future bounds that could be reached in the $(m_a[\text{eV}], g_{a\gamma\gamma}[\text{GeV}^{-1}])$ plane assuming a fiducial PUCH (dot-dashed) (FG (dashed)) reionization model and a 1σ error on τ reduced to 0.005 (0.002). Other continuous colored lines correspond to existing limits from a conservative Leo-T analysis [16] (blue), a previous CMB analysis [12] (green) and X-ray limits [11] (cyan).

could be improved and reach $\sigma(\tau) = 0.002$, very close to the cosmic variance limit (CVL) [41]. These values have to be compared to $\sigma_{\text{Pl}}(\tau) = 0.007$ from Planck 2018 [1]. One can then estimate how the constraints shown in Fig. 4 would improve with future CMB experiments by considering the improved sensitivities on the determination of the optical depth. Here we impose $\tau < \tau_{\text{Pl}} + 2 \times \sigma_{\text{fut}}(\tau)$, i.e. assuming that the central value of τ would not change but the error would be decreased to $\sigma_{\text{fut}}(\tau) < \sigma_{\text{Pl}}(\tau)$. The resulting forecasts are shown in Fig. 5. Considering $\sigma_{\text{fut}}(\tau) = 0.002$, the CMB bound assuming a FG reionization (dashed orange line) could become at least as strong as the current PUCH limit with $\sigma_{\text{Pl}}(\tau) = 0.007$. This implies that with CMB-S4 & kSZ, the bound arising from CMB anisotropies could become as good as the one from the Leo-T gas temperature [16], even in the more conservative reionization model considered here (FG). We have also checked that the CVL relative uncertainty $\sigma(\tau)/\tau = 2.5\%$ [42] does not lead to significant change in the limit and the resulting sensitivity is essentially superposed to the $\sigma(\tau) = 0.002$ case. Very interestingly, in the case of a reionization model such as the PUCH one, basically any improvement in the precision of the optical depth to reionization will improve upon the Leo-T bound. Furthermore, we also show in Fig. 5 the estimate of the limit for a modest improvement from $\sigma_{\text{Pl}}(\tau) = 0.007$ to $\sigma_{\text{fut}}(\tau) = 0.005$ with a dot-dashed orange line. Such a small improvement would increase the CMB bound on $g_{a\gamma\gamma}$ by almost one order of magnitude and become the most stringent bound on this mass range.

4 Lyman- α constraints

In the previous section, we have used CMB anisotropies to constrain the effects of the DM energy injections on the ionization history. However, and as aforementioned, DM decays also affect the IGM temperature, see e.g Fig. 1 (right panel). Using recent determinations of the IGM temperature in the redshift range $3.6 < z < 5.8$ from Lyman- α data [2, 3], the authors of Ref. [17] derived constraints on the mass and coupling to photons of DM particles with masses above 10 keV. They have used the TIGM branch of the DarkHistory code, where they implemented a modified chi-square test that only penalizes temperature histories that overheat the IGM compared to the data. In this section, we

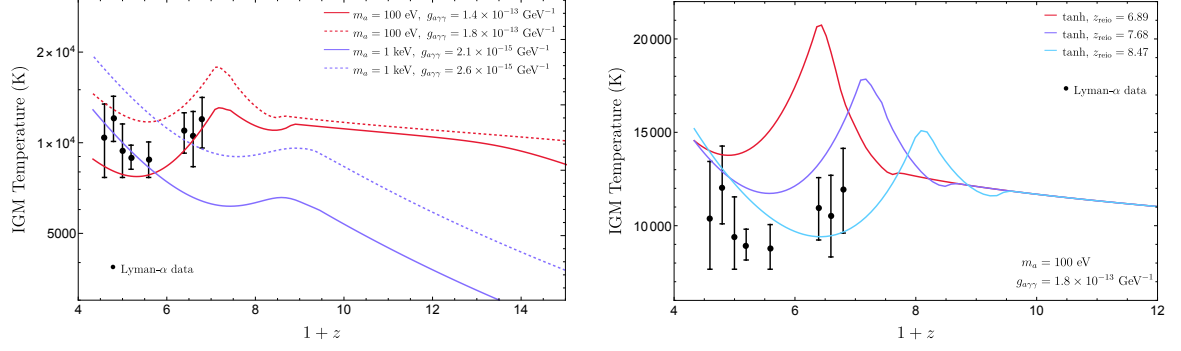


Figure 6. Evolution of the IGM temperature. Left panel: Solid lines depict the evolution for values of the coupling to photons compatible with Lyman-alpha data from [2, 3] and whereas dashed lines correspond to values incompatible with the same data. The ionization fraction has been fixed to the tanh model with $z_{\text{reio}} = 6.89$. Right panel: Same temperature evolution as in the left panel but for fixed DM mass and coupling to photons and three different values of z_{reio} .

extend such an analysis down to DM masses of 30 eV, using our modified version of the TIGM branch of the DarkHistory code.¹²

The analysis of Ref. [17] includes conservative assumptions concerning the astrophysical sources of heating and ionization. On the one hand, the astrophysical source for photoheating is set to zero ($\mathcal{H}_X^{\gamma\text{-heat}} = 0$ in Eq. (2.11)) whereas a minimal astrophysical HI photoionization rate, denoted by $\Gamma_{\text{HI}}^{\gamma\text{-ion}}$ in Eq. (2.11), is considered.¹³ The latter is obtained by requiring that all the contributions to the ionized fraction sum up, at small redshifts (from the onset of reionization until today) to the hyperbolic tangent model discussed in Sec. 2.3.1 with a z_{reio} within 1σ of the central value of Planck 2018 data.¹⁴ In practice, one imposes

$$\dot{x}_{\text{HII}}^{\text{astro}} = \frac{\dot{x}_e^{\text{tanh}}}{1 + \mathcal{F}_{\text{He}}} - \dot{x}_{\text{HII}}^{\text{DM}} - \dot{x}_{\text{HII}}^{(0)}, \quad (4.1)$$

where it has been assumed that Hydrogen and Helium have similar ionized fractions so that $x_{\text{HII}}^{\text{tanh}} = x_e^{\text{tanh}}/(1 + \mathcal{F}_{\text{He}})$, with $\mathcal{F}_{\text{He}} = n_{\text{HeII}}/n_{\text{H}}$ the ratio of singly ionized Helium to Hydrogen atoms.

In the left panel of Fig. 6, we show the evolution of the IGM temperature for DM masses of 100 eV (red) and 1 keV (blue) in the redshift range $3 < z < 14$ assuming a tanh reionization model with $z_{\text{reio}} = 7.68$. As expected, for shorter lifetimes (dashed curves) the effects of DM energy injection cause earlier and stronger heating of the IGM when compared to the case of longer lifetimes (solid curves). Following the modified chi-squared test described in the first paragraph of this section, the former cases are excluded by the IGM temperature data at 95%CL whereas the latter ones are still compatible with the data.¹⁵ On the other hand, when increasing the DM mass, we find that the heating starts at a later time but grows at a faster pace.

In the right plot of Fig. 6, we fix the DM mass and lifetime and show instead the dependence of the IGM temperature evolution on the parameter z_{reio} that controls the time of reionization in the tanh model. We show the evolution for z_{reio} between 6.89 (red) and 8.47 (cyan), corresponding to the values at 1σ around the Planck 2018 central value $z_{\text{reio}} = 7.68$ (blue) [1]. Note also the presence of a peak at a redshift around $z = z_{\text{reio}}$. The peak occurs at a smaller redshift when reionization happens

¹²We have modified all branches of the DarkHistory code to include collisional excitation processes at higher redshifts, before the onset of reionization, see the discussion in appendix B.

¹³This branch of the code also neglects the ionization of HeII to HeIII. This is justified for redshifts prior to the full ionization of HeII ($z \sim 3$ [43]) which is the case in this section where all data points are at redshifts above $z \sim 3.6$.

¹⁴In [17] two different parametrizations of the ionization fraction were considered: the tanh model and to the so-called FlexKnot parameterization that is also used in the Planck analysis [1]. We verified that our bounds are similar for both models so, for simplicity, we restrict ourselves to the tanh case in this work.

¹⁵We follow the same prescription as in [17] and discard two of the Lyman- α data points of Ref. [2].

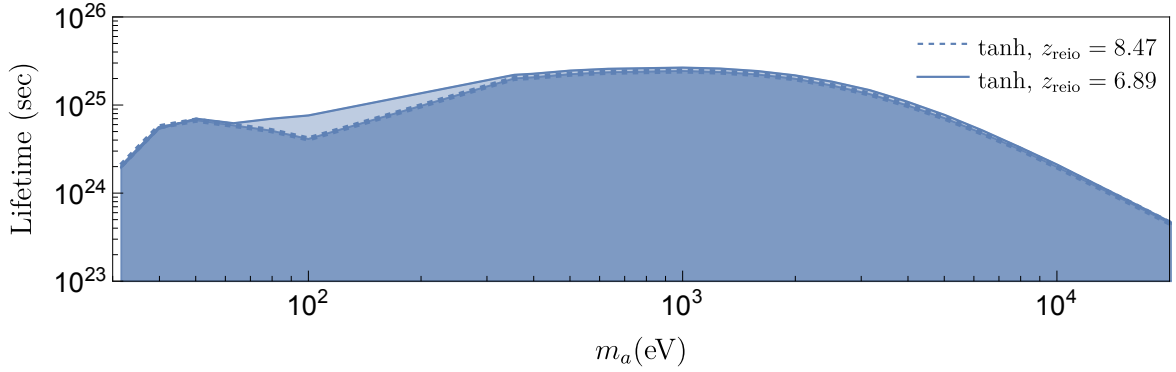


Figure 7. *Constraints on the lifetime of DM decay to two photons from IGM temperature data at 95%CL assuming a tanh model for the ionized fraction. The lighter (darker) contours refers to reionization histories that start at a redshift 1σ above (below) the central value measured by Planck 2018 data.*

later (smaller z_{reio}). From this plot, it appears that an earlier reionization is easier to comply with the Lyman- α data.

We have then performed a systematic analysis to find the DM parameters ($m_a, g_{a\gamma\gamma}$) that are excluded by the Lyman- α data at 95%CL due to overheating of the IGM temperature. In Fig. 7 we present these bounds in terms of the DM mass and lifetime, which is equal to Γ_{dec}^{-1} with Γ_{dec} given by Eq. (2.5), and their dependence on z_{reio} . In the mass range between 30 eV to 1 keV we obtain bounds on the lifetime between 2×10^{24} and 2×10^{25} seconds. The bounds are stronger for late reionizations and can differ by up to a factor of three, for masses ~ 100 eV, between the largest and smallest z_{reio} consider in this work. This can be traced back to the small bump in temperature arising at the onset of reionization and that is well visible in Fig. 6. There we see that for late reionization scenarios this small increase in temperature is probed by the Lyman- α data, while for earlier reionizations the bump happens at larger redshifts where there is no data yet. Furthermore, we find that the bump is more prominent for DM masses around 100 eV thus causing the biggest difference at those masses.

Finally, in order to compare the Lyman- α bounds obtained here to the ones from the CMB analysis derived in the previous section, we project in Fig. 4, the most stringent constraint on the lifetime shown in Fig. 7 (for $z_{\text{reio}} = 6.89$) with a continuous yellow line. As we see, the very conservative assumption made here on the heating of the IGM in a tanh model gives rise to a bound that can readily compete with the previous CMB bounds from Ref. [12] for $m_a \gtrsim 200$ eV. They can however not compete with the most recent CMB bounds derived in Sec. 3.

5 Conclusion

The ionization history and the evolution of the IGM temperature are known to be very sensitive to DM injections of energy and can be tested via CMB anisotropies and Lyman- α data. In this work, we have used Planck 2018 data and recent determinations of the IGM temperature at low redshifts, to update and extend previous constraints on the decay to photons of DM particles with masses between 20.4 eV (two times the Lyman- α threshold) and ~ 1 keV (where X-ray bounds kick in, see [11]). To derive these constraints, we relied on the **DarkHistory** v1.1 code [13] that calculates the energy deposition efficiencies as a function of the redshift, for any type of exotic injection source and deposition channel, and self-consistently computes the corresponding evolution of the Hydrogen and Helium ionized fractions and the IGM temperature. These quantities can then be used to compute constraints from CMB, Lyman- α or e.g. future 21-cm data.

The ionized fractions and the IGM temperature are sensitive to the astrophysical model which drives reionization. In Sec. 2, we have briefly described how in practice energy injection from DM and astrophysics is implemented in **DarkHistory**. We have commented on some modifications that we have introduced for our analysis. First, we take into account cooling due to collisional excita-

tion processes at redshifts above reionization (see Sec. 2.3 and App. B). The latter appears to have an important effect on the evolution of the IGM temperature for the DM masses and lifetimes range considered in this work. Second, in order to study the dependence of the evolution of the IGM temperature and the ionized fractions on the astrophysical model for the photoheating and photoionization rates, we have considered the FG model [14] in addition to the default tanh and PUCH [15] models implemented in **DarkHistory**. While the hyperbolic tangent model allows to easily marginalize over several reionization histories, it does not however predict a unique IGM temperature evolution. On the other hand, the FG and PUCH astrophysics models for reionization allow to self-consistently account for ionization and heating at low redshifts via both DM and astrophysical contributions.

In Sec. 3, we have derived new constraints on ALP decays into two photons considering the three reionization models mentioned above. For that purpose, we have modified **CLASS** to interpolate the reionization histories at low redshifts and the effective energy deposition efficiencies at higher redshifts over the DM masses and coupling to photons considered in this work. The effective energy deposition efficiencies were taken to be constant in time and equal to $f_c(x_e, z = 300)$ following the findings of [33]. We then performed an MCMC analysis including the baseline TT,TE,EE and low E Planck 2018 likelihoods and ran over a set of cosmological parameters including the DM mass and coupling to photons as well as the reionization redshift when considering a tanh model. Compared with previous works [11, 12], our analysis improves the bounds on the DM lifetime by exploiting the full CMB anisotropy spectrum information of the latest Planck data release, and explores for the first time their dependence on the astrophysical models for reionization using the self-consistent evaluation of x_e .

The summary plot of all our results is provided in Fig. 4. In particular, the three red lines delimit the regions on the ALP parameter space (mass and coupling to photons) that are excluded at 99%CL for the three reionization models that we have considered. Note however that, by properly re-expressing the bounds on $g_{a\gamma\gamma}$ in terms of the DM lifetime, our constraints apply to any other DM model decaying to two photons. The limits are slightly more stringent in the case of the PUCH model [15]. This is expected as in the latter case the optical depth to reionization in the absence of DM energy injections is already significantly larger than the central value obtained with Planck 2018 and a tanh model. Overall, the CMB bounds obtained here are competitive with previous existing constraints in the mass range from 20.4 eV to 400 eV, except for the Leo-T bound from [16]. Let us emphasize though that the Leo-T and CMB bounds are independent as they rely on very different astrophysical and cosmological phenomena and assumptions. The CMB analysis has the advantage that it mostly relies on the linear evolution of the cosmological perturbations, which is well understood. However, it also partly inherits the astrophysical uncertainties on the reionization history as we show explicitly in our analysis with the three different reionization models. In Fig. 5, we have estimated the sensitivity of future CMB surveys and concluded that the latter shall give rise to constraints competitive with the Leo-T bound, even in the most conservative reionization scenarios. In the future, it would be interesting to go beyond the two specific reionization models from stars considered in this work and simultaneously constrain the models by CMB, Lyman- α and UV and X-ray data.

Finally, in Sec. 4, we have focused on the evolution of the IGM temperature. The recent advancements in hydrodynamical simulations and in the measurements of Lyman- α data have allowed a determination of the IGM temperature at redshifts $z < 7$. These data have been used in [17] to set bounds on the decay rate to photons of DM particles with masses above 10 keV. Here we have extended this analysis to lower masses taking care of accounting for the cooling from collisional excitations processes in the high redshift range, before the onset of reionization. Assuming a tanh model for the ionized fractions, our final constraints on the DM lifetime are illustrated in Fig. 7 with two different reionization redshifts that correspond to the $\pm 1\sigma$ values around the central value obtained from the Planck 2018 data. The most stringent of these bounds is also reported in Fig. 4 with a yellow line to ease the comparison with the CMB limits. It appears that, given the methodology followed here, the Lyman- α bounds are up to one order of magnitude weaker than the CMB bounds obtained in Sec. 3. Note, however, that the Lyman- α data has the advantage that it provides tomographic constraints, i.e. at different redshifts, on the dark matter injection of energy whereas the CMB data

is most sensitive to the integrated effect of the DM energy injection, through the parameter τ as we discussed in the main text. It would however be interesting to review these constraints in the light of next-generation measurements of 21 cm emission/absorption that is expected to become a very sensitive probe of the IGM temperature at low redshifts, see e.g. [44], and potentially surpass the CMB constraint for DM decay, see also [23, 45–47].

Note Added: Upon the completion of this work, we became aware of the work in [48, 49] on a new version of the `DarkHistory` code that improves on the treatment of low-energy particles and in particular estimates the CMB constraints on the DM parameters. Their results show that the new version of the code does not affect significantly the CMB constraints derived in Sec. 3.

Acknowledgements

We thank M. Lucca, D.C. Hooper and N. Schoeneberg for discussions and support on dealing with DM energy injection and reionization in `CLASS` and `MontePython`. We also thank T. Slatyer and H. Liu for clarifications on `DarkHistory`. Furthermore, we acknowledge useful discussions with J. Torrado. LLH is supported by the Fonds de la Recherche Scientifique F.R.S.-FNRS through a research associate position and acknowledges support of the FNRS research grant number F.4520.19, the ARC program of the Federation Wallonie-Bruxelles and the IISN convention No. 4.4503.15. Computational resources have been provided by the Consortium des Equipements de Calcul Intensif (CECI), funded by the Fonds de la Recherche Scientifique de Belgique (F.R.S.-FNRS) under Grant No. 2.5020.11 and by the Walloon Region of Belgium. RZF is supported by the Direcció General de Recerca del Departament d’Empresa i Coneixement (DGR) and by the EC through the program Marie Skłodowska-Curie COFUND (GA 801370)-Beatriu de Pinós and partially by the FCT grant No. CERN/FIS-PAR/0027/2021. This work has been partially supported by the MCIN/AEI/10.13039/501100011033 of Spain under grant PID2020-113644GB-I00, by the Generalitat Valenciana of Spain under the grant PROMETEO/2019/083 and by the European Union’s Framework Programme for Research and Innovation Horizon 2020 (2014–2020) under grant H2020-MSCA-ITN-2019/860881-HIDDeN.

A Rates

In this appendix, we provide some more details on the ionization and heating rates contributing to the IGM temperature and ionized fractions evolutions discussed in Sec. 2. A more complete list of these rates can be found for example in [13, 17, 20, 21].

Let us first discuss the contribution to the term $\dot{Y}^{(0)}$ of Eq. (2.1). As discussed in Sec. 2.1, there are ionization processes (\dot{x}_X^{ion}) that increase the number of free electrons and recombination processes (\dot{x}_X^{rec}) that have the opposite effect. Depending on the redshift of the process, there are two different regimes: case-B for optically thin medium, applicable at redshifts larger than the onset of reionization z_A^{max} when the universe is mostly neutral, and case-A for optically thick medium, that applies for small redshifts $z \lesssim z_A^{\text{max}}$ after reionization starts.

In the optically thick regime, case-A, recombination and ionization via collisional ionization are the leading processes included in `DarkHistory`. In this case, Eq. (2.3) is given by [17, 20, 21]:

$$\begin{pmatrix} \dot{x}_{\text{HII}}^{(0)} \\ \dot{x}_{\text{HeII}}^{(0)} \\ \dot{x}_{\text{HeIII}}^{(0)} \end{pmatrix} = n_e \begin{pmatrix} (1 - x_{\text{HII}})\Gamma_{\text{HI}}^{\text{col-ion}} - x_{\text{HII}}\alpha_{\text{HI}}^A \\ (\mathcal{F}_{\text{He}} - x_{\text{HeII}} - x_{\text{HeIII}})\Gamma_{\text{HeI}}^{\text{col-ion}} + x_{\text{HeIII}}\alpha_{\text{HeIII}}^A - x_{\text{HeII}}(\Gamma_{\text{HeII}}^{\text{col-ion}} + \alpha_{\text{HeII}}^A) \\ x_{\text{HeII}}\Gamma_{\text{HeIII}}^{\text{col-ion}} - x_{\text{HeIII}}\alpha_{\text{HeIII}}^A \end{pmatrix}. \quad (\text{A.1})$$

where $\Gamma_X^{\text{col-ion}}$ are the collisional ionization rates of the different species, given e.g. in [20], and α_X^A is the case-A recombination coefficient. Note that, the photoionization processes are expected to be dominated by the astrophysical sources during reionization and so are not included in $\dot{Y}^{(0)}$ but rather in the astro-term \dot{Y}^{astro} of Eq. (2.1), see Sec. 2.3.

In the optically thin regime, case-B, the processes that are instead taken into account in **DarkHistory** are recombination and photoionizations given by **DarkHistory** [13]

$$\begin{pmatrix} \dot{x}_{\text{HII}}^{(0)} \\ \dot{x}_{\text{HeII}}^{(0)} \end{pmatrix} = \begin{pmatrix} \mathcal{C}_{\text{H}} [4(1 - x_{\text{HII}})\beta_{\text{H}}^B e^{E_{21}/T_{\text{CMB}}} - n_{\text{H}}x_e x_{\text{HII}}\alpha_{\text{H}}^B] \\ \sum_{i=s,t} \mathcal{C}_{\text{He}^i} [g_i(\mathcal{F}_{\text{He}} - x_{\text{HeII}})\beta_{\text{He}^i}^B e^{-E_{\text{He}^i}/T_{\text{CMB}}} - n_{\text{H}}x_e x_{\text{HeII}}\alpha_{\text{He}^i}^B] \end{pmatrix}, \quad (\text{A.2})$$

where $x_e = n_e/n_H$ is the electron fraction with n_e the density of free electrons and $E_{21} = 10.2$ eV is the energy of the Lyman- α transition. Also, α_X^B, β_X^B are the case-B recombination and photoionization coefficients. \mathcal{C}_X is the Peebles-C factor for the species $X=\{\text{Hydrogen (H)}, \text{ and singlet (s) and triplet (t) Helium (He}^{s,t})\}$, i.e. the probability for the species X in the $n = 2$ state to decay to the ground state, and g_i is the multiplicity of the state $i = s, t$ and $\mathcal{F}_{\text{He}} = n_{\text{He}}/n_H$. Note that, in **DarkHistory** the doubly-ionized Helium (HeIII) is only taken into account during reionization (case-A), where it is expected to be non-negligible, but not before (case-B).

Finally, the \dot{Y}^{DM} term of Eq. (2.7) accounts for the contributions from DM energy injection. The prefactor A introduced in Eq. (2.7) takes the form [13]:

$$A = \begin{pmatrix} \frac{2f_{\text{heat}}}{3(1+\mathcal{F}_{\text{He}}+x_e)} \\ \frac{1}{\mathcal{R}_{\text{HI}}} (f_{\text{HII}} + \frac{4}{3}(1 - \mathcal{C}_{\text{H}})f_{\text{exc}}) \\ \frac{f_{\text{HeII}}}{\mathcal{R}_{\text{HeI}}} \\ \frac{f_{\text{HeIII}}}{\mathcal{R}_{\text{HeII}}} \end{pmatrix} \quad (\text{A.3})$$

where \mathcal{R}_X is the ionization potential of the atom/ion X.

B Modified DarkHistory

While running **DarkHistory** for sub-keV masses we observed a sudden drop of the matter temperature at redshifts near the beginning of reionization. We found the effect to be more prominent for DM masses around 100 eV and couplings $g_{a\gamma\gamma}$ larger than a few times $10^{-13} \text{ GeV}^{-1}$. We noticed that this drop is much less significant when considering larger masses for the decaying DM.

It appears that the origin of this sudden drop is related to the (non-)inclusion of collisional excitations at redshifts around the onset of reionization, that we denote with z_A^{max} , in both the **TIGM** and **Master** branches of **DarkHistory** used here. These processes have the largest cooling rates at the threshold of reionization (at least for the DM masses and couplings mentioned above) and they are included for $z < z_A^{\text{max}}$ (in the reionization part of the code) by default, with e.g. $z_A^{\text{max}} = 15.1$ for the PUCH model. If we do not include such processes for $z > z_A^{\text{max}}$, we get a sudden drop in T_m at the matching point. We have modified the *tla.py* file, which includes the evolution of the matter temperature so that the collisional excitation terms are also included before the matching. We have done so in both the **Master** (used in Secs 2.3 and 3) and **TIGM** (used in Sec. 4) branches of the **DarkHistory v1.1** code. Using this modified version, the sudden drop in the matter temperature disappeared without changing the pre-reionization evolution. The temperature drop can also have, indirectly, a significant impact on the ionization history when dark matter energy injection is relatively large. However, we find that the x_e evolution is very weakly affected for ALP masses and couplings at the limit of our exclusion bounds obtained in our CMB analysis, see Sec. 3.2. This can be seen in Fig. 8, which shows a comparison between the reionization history obtained using the original version of the code (continuous lines) and our modified version (dashed lines), assuming $m_a = 100$ eV. In the top panels we use the PUCH model with $z_A^{\text{max}} = 15.1$, whereas in the bottom panels, the FG rates are employed with $z_A^{\text{max}} = 7.8$. The sudden drop obtained with the original code around z_A^{max} disappears with our modifications. We have also tested how the inclusion of additional cooling/heating terms in the pre-reionization evolution, such as collisional ionization and bremsstrahlung, would affect the results but we did not find sizeable effects, which can be understood from the fact that these rates are subdominant.

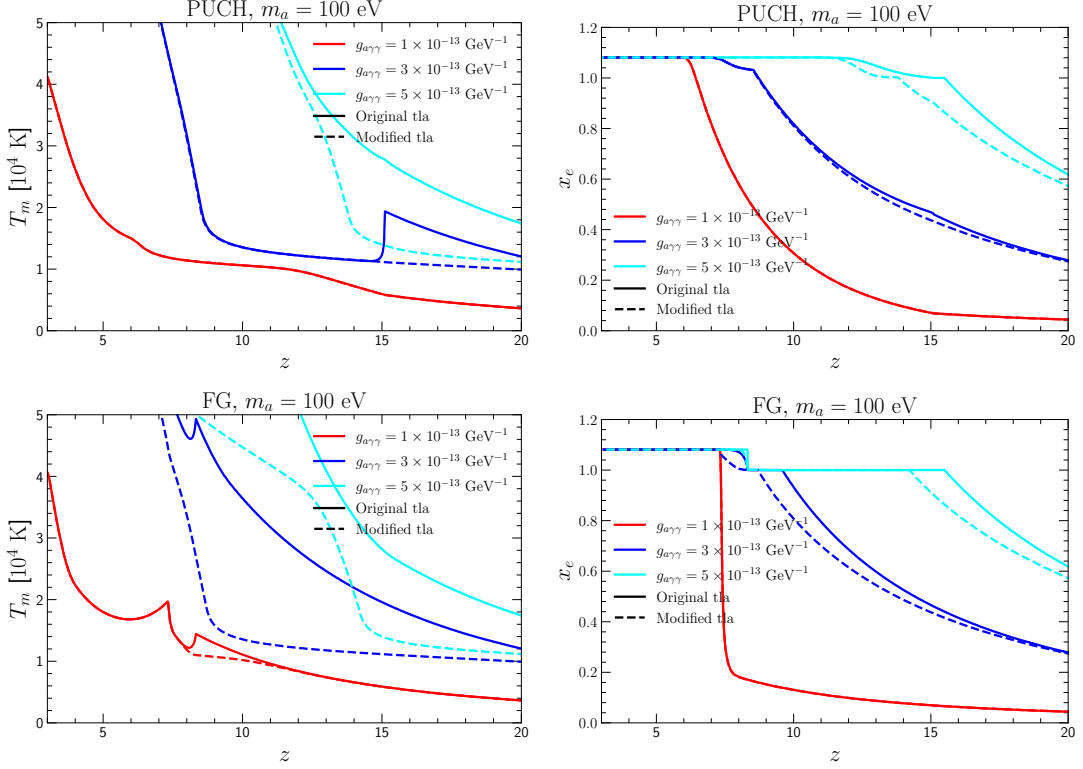


Figure 8. Comparison between the reionization history obtained using the original version of **DarkHistory** (continuous lines) and our modified version (dashed lines), in terms of the matter temperature T_m (left panel) and ionization fraction x_e (right panel). The reionization history in the top panels is obtained using PUCH, whereas FG is employed for the bottom panels.

References

- [1] PLANCK collaboration, *Planck 2018 results. VI. Cosmological parameters*, *Astron. Astrophys.* **641** (2020) A6 [[1807.06209](#)].
- [2] M. Walther, J. Oñorbe, J.F. Hennawi and Z. Lukić, *New Constraints on IGM Thermal Evolution from the Ly α Forest Power Spectrum*, *Astrophys. J.* **872** (2019) 13 [[1808.04367](#)].
- [3] P. Gaikwad et al., *Probing the thermal state of the intergalactic medium at $z > 5$ with the transmission spikes in high-resolution Ly α forest spectra*, *Mon. Not. Roy. Astron. Soc.* **494** (2020) 5091 [[2001.10018](#)].
- [4] F. Takahashi and W. Yin, *Challenges for heavy QCD axion inflation*, *JCAP* **10** (2021) 057 [[2105.10493](#)].
- [5] G.B. Gelmini, A. Simpson and E. Vitagliano, *Gravitational waves from axionlike particle cosmic string-wall networks*, *Phys. Rev. D* **104** (2021) 061301 [[2103.07625](#)].
- [6] J.L. Bernal, A. Caputo, G. Sato-Polito, J. Mirocha and M. Kamionkowski, *Seeking dark matter with γ -ray attenuation*, [2208.13794](#).
- [7] N.P. Branco, R.Z. Ferreira and J.a.G. Rosa, *Superradiant axion clouds around asteroid-mass primordial black holes*, [2301.01780](#).
- [8] P. Carenza, G. Lucente and E. Vitagliano, *Probing the Blue Axion with Cosmic Optical Background Anisotropies*, [2301.06560](#).
- [9] T.R. Slatyer, *Indirect dark matter signatures in the cosmic dark ages. I. Generalizing the bound on s -wave dark matter annihilation from Planck results*, *Phys. Rev. D* **93** (2016) 023527 [[1506.03811](#)].

- [10] T.R. Slatyer, *Indirect Dark Matter Signatures in the Cosmic Dark Ages II. Ionization, Heating and Photon Production from Arbitrary Energy Injections*, *Phys. Rev. D* **93** (2016) 023521 [[1506.03812](#)].
- [11] D. Cadamuro and J. Redondo, *Cosmological bounds on pseudo Nambu-Goldstone bosons*, *JCAP* **02** (2012) 032 [[1110.2895](#)].
- [12] B. Bolliet, J. Chluba and R. Battye, *Spectral distortion constraints on photon injection from low-mass decaying particles*, *Mon. Not. Roy. Astron. Soc.* **507** (2021) 3148 [[2012.07292](#)].
- [13] H. Liu, G.W. Ridgway and T.R. Slatyer, *Code package for calculating modified cosmic ionization and thermal histories with dark matter and other exotic energy injections*, *Phys. Rev. D* **101** (2020) 023530 [[1904.09296](#)].
- [14] C.-A. Faucher-Giguère, *A cosmic UV/X-ray background model update*, *Mon. Not. Roy. Astron. Soc.* **493** (2020) 1614 [[1903.08657](#)].
- [15] E. Puchwein, F. Haardt, M.G. Haehnelt and P. Madau, *Consistent modelling of the meta-galactic UV background and the thermal/ionization history of the intergalactic medium*, *Mon. Not. Roy. Astron. Soc.* **485** (2019) 47 [[1801.04931](#)].
- [16] D. Wadekar and Z. Wang, *Strong constraints on decay and annihilation of dark matter from heating of gas-rich dwarf galaxies*, *Phys. Rev. D* **106** (2022) 075007 [[2111.08025](#)].
- [17] H. Liu, W. Qin, G.W. Ridgway and T.R. Slatyer, *Lyman- α constraints on cosmic heating from dark matter annihilation and decay*, *Phys. Rev. D* **104** (2021) 043514 [[2008.01084](#)].
- [18] P.J.E. Peebles, *Recombination of the Primeval Plasma*, *Astrophys. J.* **153** (1968) 1.
- [19] Y.B. Zeldovich and R.A. Sunyaev, *The Interaction of Matter and Radiation in a Hot-Model Universe*, *Astrophys. Space Sci.* **4** (1969) 301.
- [20] T. Theuns, A. Leonard, G. Efstathiou, F.R. Pearce and P.A. Thomas, *P**3M-SPH simulations of the Lyman-alpha forest*, *Mon. Not. Roy. Astron. Soc.* **301** (1998) 478 [[astro-ph/9805119](#)].
- [21] J.S. Bolton and M.G. Haehnelt, *The nature and evolution of the highly ionized near-zones in the absorption spectra of $z \sim 6$ quasars*, *Mon. Not. Roy. Astron. Soc.* **374** (2007) 493 [[astro-ph/0607331](#)].
- [22] T.R. Slatyer, N. Padmanabhan and D.P. Finkbeiner, *CMB Constraints on WIMP Annihilation: Energy Absorption During the Recombination Epoch*, *Phys. Rev. D* **80** (2009) 043526 [[0906.1197](#)].
- [23] L. Lopez-Honorez, O. Mena, S. Palomares-Ruiz and A.C. Vincent, *Constraints on dark matter annihilation from CMB observations before Planck*, *JCAP* **07** (2013) 046 [[1303.5094](#)].
- [24] V. Poulin, P.D. Serpico and J. Lesgourgues, *Dark Matter annihilations in halos and high-redshift sources of reionization of the universe*, *JCAP* **12** (2015) 041 [[1508.01370](#)].
- [25] J. Lesgourgues, *The Cosmic Linear Anisotropy Solving System (CLASS) I: Overview*, [1104.2932](#).
- [26] D. Blas, J. Lesgourgues and T. Tram, *The Cosmic Linear Anisotropy Solving System (CLASS) II: Approximation schemes*, *JCAP* **07** (2011) 034 [[1104.2933](#)].
- [27] J. Lesgourgues and T. Tram, *Fast and accurate CMB computations in non-flat FLRW universes*, *JCAP* **09** (2014) 032 [[1312.2697](#)].
- [28] A. Lewis, *Cosmological parameters from WMAP 5-year temperature maps*, *Phys. Rev. D* **78** (2008) 023002 [[0804.3865](#)].
- [29] J.M. Shull and M.E. van Steenberg, *X-ray secondary heating and ionization in quasar emission-line clouds*, *Astrophys. J.* **298** (1985) 268.
- [30] X.-L. Chen and M. Kamionkowski, *Particle decays during the cosmic dark ages*, *Phys. Rev. D* **70** (2004) 043502 [[astro-ph/0310473](#)].
- [31] N. Padmanabhan and D.P. Finkbeiner, *Detecting dark matter annihilation with CMB polarization: Signatures and experimental prospects*, *Phys. Rev. D* **72** (2005) 023508 [[astro-ph/0503486](#)].
- [32] R. Diamanti, L. Lopez-Honorez, O. Mena, S. Palomares-Ruiz and A.C. Vincent, *Constraining Dark Matter Late-Time Energy Injection: Decays and P-Wave Annihilations*, *JCAP* **02** (2014) 017 [[1308.2578](#)].

- [33] T.R. Slatyer and C.-L. Wu, *General Constraints on Dark Matter Decay from the Cosmic Microwave Background*, *Phys. Rev. D* **95** (2017) 023010 [[1610.06933](#)].
- [34] J. Lesgourgues, *The cosmic linear anisotropy solving system (class) i: Overview*, 2011. 10.48550/ARXIV.1104.2932.
- [35] P. Stöcker, M. Krämer, J. Lesgourgues and V. Poulin, *Exotic energy injection with ExoCLASS: Application to the Higgs portal model and evaporating black holes*, *JCAP* **03** (2018) 018 [[1801.01871](#)].
- [36] M. Lucca, N. Schöneberg, D.C. Hooper, J. Lesgourgues and J. Chluba, *The synergy between CMB spectral distortions and anisotropies*, *JCAP* **02** (2020) 026 [[1910.04619](#)].
- [37] Y. Ali-Haïmoud and C.M. Hirata, *Ultrafast effective multi-level atom method for primordial hydrogen recombination*, *Phys. Rev. D* **82** (2010) 063521 [[1006.1355](#)].
- [38] N. Lee and Y. Ali-Haïmoud, *HYREC-2: a highly accurate sub-millisecond recombination code*, *Phys. Rev. D* **102** (2020) 083517 [[2007.14114](#)].
- [39] D.P. Finkbeiner, S. Galli, T. Lin and T.R. Slatyer, *Searching for Dark Matter in the CMB: A Compact Parameterization of Energy Injection from New Physics*, *Phys. Rev. D* **85** (2012) 043522 [[1109.6322](#)].
- [40] T. Brinckmann and J. Lesgourgues, *MontePython 3: boosted MCMC sampler and other features*, *Phys. Dark Univ.* **24** (2019) 100260 [[1804.07261](#)].
- [41] K. Abazajian et al., *CMB-S4 Science Case, Reference Design, and Project Plan*, [1907.04473](#).
- [42] D.J. Watts et al., *A Projected Estimate of the Reionization Optical Depth Using the CLASS Experiment’s Sample Variance Limited E-mode Measurement*, *Astrophys. J.* **863** (2018) 121 [[1801.01481](#)].
- [43] G.D. Becker, J.S. Bolton, M.G. Haehnelt and W.L.W. Sargent, *Detection of Extended He II Reionization in the Temperature Evolution of the Intergalactic Medium*, *Mon. Not. Roy. Astron. Soc.* **410** (2011) 1096 [[1008.2622](#)].
- [44] H. Liu and T.R. Slatyer, *Implications of a 21-cm signal for dark matter annihilation and decay*, *Phys. Rev. D* **98** (2018) 023501 [[1803.09739](#)].
- [45] S.R. Furlanetto, S.P. Oh and E. Pierpaoli, *The Effects of Dark Matter Decay and Annihilation on the High-Redshift 21 cm Background*, *Phys. Rev. D* **74** (2006) 103502 [[astro-ph/0608385](#)].
- [46] M. Valdes, A. Ferrara, M. Mapelli and E. Ripamonti, *Constraining DM through 21 cm observations*, *Mon. Not. Roy. Astron. Soc.* **377** (2007) 245 [[astro-ph/0701301](#)].
- [47] C. Evoli, A. Mesinger and A. Ferrara, *Unveiling the nature of dark matter with high redshift 21 cm line experiments*, *JCAP* **11** (2014) 024 [[1408.1109](#)].
- [48] H. Liu, W. Qin, G.W. Ridgway and T.R. Slatyer, *Exotic energy injection in the early universe I: a novel treatment for low-energy electrons and photons*, [2303.07366](#).
- [49] H. Liu, W. Qin, G.W. Ridgway and T.R. Slatyer, *Exotic energy injection in the early universe II: CMB spectral distortions and constraints on light dark matter*, [2303.07370](#).